

Materials selection for XL wind turbine support structures: A corrosion-fatigue perspective



Victor Igwemezie, Ali Mehmanparast*, Athanasios Kolios

Offshore Energy Engineering Centre, Cranfield University, Cranfield, Bedfordshire, England, UK

ARTICLE INFO

Keywords:

Offshore wind turbine
Fatigue
Corrosion-fatigue
Fatigue crack growth
Seawater
S355
Steel
BS7910

ABSTRACT

The continued growth of the offshore wind industry will depend essentially on reductions in wind energy production cost. Large cost reductions can be achieved through efficient, economic and optimised wind turbine support structures. To achieve maximum offshore wind adoption beyond 2020, significant industrial and research efforts are being made in optimised material selection and application. Fatigue and corrosion damage are the greatest challenges today in design and life estimation of wind turbine support structures. S355 steel is currently used in fabrication of most wind turbine monopile support structures. Clear understanding of their corrosion-fatigue properties and accurate steel selection will support the optimisation and economic design of extra-large wind turbines. This paper presents the fatigue crack growth test results of advanced S355 TMCP steel in air and seawater, and compares the results with studies on commonly available S355 steel. The results show that S355 TMCP steels generally offer higher fatigue damage tolerance than normalised S355 steels in air and the factor decreases and tends towards a common value with increase in stress intensity factor range. However, in seawater there is no significant difference in fatigue crack growth rates for all the S355 ferritic steels considered in this study.

1. Introduction

The growth of the offshore wind industry will depend essentially on reductions in wind energy cost. Experience with the technology has revealed that environmentally friendly and economical wind energy can be produced by increasing the size of the turbine [1]. This simply means that the larger the turbine, the greener the electricity [2]. Consequently, offshore wind turbines (OWTs) are growing larger because of the need to push down the total cost of wind energy to a minimum. Previous studies have shown that further cost reduction could be achieved through efficient, economic and optimised turbine support structure, the dominant being the monopiles [3]. In the last few years, Levelised Cost of Energy (LCOE) target of £100/MWh was set to be achieved by 2020 [4]. In 2016, it was reported that the target of £100/MWh for offshore wind has been achieved 4 years before the target date [5]. The reduction was reported to be from £142/MWh to £97/MWh for UK projects reaching FID in 2015/16. Currently, Scotland has planned to add 1 GW in wind energy capacity. *Scottish Renewables*, the representative of the Scottish renewable energy industry, will be auctioning the new capacity from 2018/19 with clearing price expected to be £49.4/MWh in real 2017 terms [6].

Monopiles are the most commonly used wind turbine support structure due to their simplicity in design compared to other foundation concepts [7,8]. At water depths up to 30 m, monopile has clearly more commercial and technical advantages. It is well-suited for mass production as the installation method is based on conventional impact driving and is robust in most soil conditions

* Corresponding author.

E-mail address: a.mehmanparast@cranfield.ac.uk (A. Mehmanparast).

Nomenclature	
a_o	Initial crack length
a_f	Final crack length
σ_y	Yield stress
σ_{UTS}	Ultimate tensile stress
$\Delta\sigma$	Cyclic stress range
ΔK	Cyclic SIFR
da/dN	Fatigue crack growth rate (m/cycle)
P_{max}	Maximum load
P_{min}	Minimum load
K	Stress intensity factor (SIF)
R	Stress ratio
$CFCGR$	Corrosion-fatigue crack growth rate
FCG	Fatigue crack growth
$FCGR$	Fatigue crack growth rate
FID	Final Investment Decision
$HAWT$	Horizontal axis wind turbine
$LEFM$	Linear Elastic Fracture Mechanics
OWT	Offshore WT
$SLIC$	Structural Lifecycle Industry Collaboration Joint Industry Project
$SIFR$	Stress intensity factor range
SW	Seawater
$TMCP$	Thermo-mechanically control process
WT	Wind turbine
XL	Extra Large
PS	Present study

[3]. The literature has shown that the dominant majority of the commissioned offshore wind structures currently in use are supported by monopile structures while less than 10% are supported on jacket structures [9]. Although, many newly licensed wind farms in Europe, especially in UK Round 3 and Germany, to be developed before 2020 are at water depths below 40m, offshore activity is progressing towards deeper waters, requiring new design concepts to be considered. Despite these changes, monopile structures are maintaining interest from developers especially for large 10 MW concept designs [10–14]. Dong Energy (now Ørsted) and MHI Vestas in 2017 celebrated the installation of the world's biggest and most powerful wind turbine off the Liverpool coast. The 8 MW WT monopile is shown in Fig. 1(a), the steel material weighing about 1300 tonnes [15], while Fig. 1(b) is Gemini windpark monopile. Fig. 1(c) is the transition piece while Fig. 1(d) is the tower. The 600 MW Gemini windpark construction began in 2015 and was officially commissioned in 2017, having a total of 150 Siemens' 4.0-MW turbines. The monopiles used had dimensions of approximately 73 m in length and up to 7 m in diameter.

In the harsh offshore environment, where wind turbines (WTs) are subjected to constant exertion of cyclic wave and wind forces, it is essential to design the offshore wind turbine foundations against fatigue failure. The ultimate aim of fatigue design tests is to ensure that engineering structures perform optimally throughout their design life. Moreover, the offshore wind turbine foundations are in direct contact with seawater, hence introducing corrosion damage in the structure. Offshore WTs are relatively new structures and their long term corrosion fatigue performance data are scarce, or simply non-existent [17]. Although, wind turbines (WTs) are coated, there are periods when the coating peels giving rise to high rate of pitting and eventual crack formation. There are also many regions of the WT that are unprotected in which cracks could nucleate and grow. The presence of cracks could cause the WT



Fig. 1. Offshore WT support structures (a) 8 MW WT monopile, (b) Gemini windpark monopile, (c) transition piece, (d) tower [15,16].

components to fail catastrophically by crack propagation at loads far less than the maximum design load, and the problem is worsened for cyclic loading (fatigue) in marine environment. For this reason, it becomes a common engineering practice to measure the tendency of cracks of particular sizes to propagate under a given stress condition. Consequently, offshore structures are inspected for presence of cracks and if they are found remedy action is taken to ensure they are free from flaws.

Fracture mechanics approach is frequently employed in the prediction of the loads at which cracks of given length will grow and cause failure. This knowledge enables safe design and aids in economic and effective preventive maintenance. There is also the need to accumulate practical data that are indispensable in validation of modelling efforts for efficient futuristic design. Due to scarcity of corrosion-fatigue data for advanced S355 steel subgrades that are currently being used to design extra-large (XL) WT support structures, this paper presents a comparative study of corrosion-fatigue characteristics of some of these steels by performing new sets of experiments and comparing the results with the existing data on other sub-grades of S355 steel.

2. Wind turbine characteristics

2.1. Fatigue loading of wind turbine and analysis approach

WTs are continuously subjected to dynamic and highly cyclic loads due to the constant exertion of wind and wave forces. This situation becomes worse if they are in a very turbulent wind climate. The components which are subjected to repeated bending stress may eventually fail by initiation and growth of cracks – in a process commonly referred to as fatigue damage. Loads causing fatigue damage originate from a variety of sources – include steady loads from high winds; wind shear, yaw error and motion; stochastic loads from turbulence; transient loads from such events as gusts, operational starts and stops loads; and resonance-induced loads from vibration of the structure. Fatigue analysis simply involves understanding how component parts of the WT would perform in withstanding continuously varying loads for a particular period of time – along the lifespan scale of the WT. DNV-RP-C203 [18] recommends the use of fatigue tests or fracture mechanics for the fatigue analyses of structures. It is noted in the Standard that shorter fatigue life is normally derived from fracture mechanics than by S-N data. This makes fracture mechanics approach appealing in engineering design due to its conservativeness. The analysis in this paper is performed using the latter approach.

2.2. Natural frequency of WTs

The natural frequency with which the tower moves is often referred to as the Eigen-frequency. The value of the natural frequency depends on the structural dimensions - height of the tower, the diameter of the support structure, the wall thickness of the tower shells; type of structural material – usually steel; the weight of the top mass - rotor blade and hub; weight of the nacelle; weight of any installation and maintenance platforms on the WT; soil-structure interaction and water depth [19–22]. The frequency distribution is a significant factor in the structural fatigue life of WT components. The assessment of the first natural frequency of the offshore wind turbine is a very important part of structural analysis. The forcing frequencies that are commonly taken into considerations are:

1. Wind spectrum,
2. Operational intervals of the rotor and
3. Wave/current spectrum.

The first natural frequency reduces for a given tower shell thickness with increasing top mass. This reduction brings its natural frequency closer to the forcing frequencies of the wind and waves and this increases the risk of occurrence of resonance. Resonance causes combination and build-up of maximum amplitudes which impacts greater stress in the structure which may exceed the allowable design stress and consequently leads to structural collapse.

The primary excitation frequency due to the rotational speed of the rotor is commonly called the 1P - in fact, 1P is the rotor frequency. The second excitation frequency of WT can be explained using Fig. 2 [17,23]. In Fig. 2, the vertical tower creates wind shade. Anytime a single blade of the rotor passes the wind shade of the vertical tower there is reduction of the wind loading on the

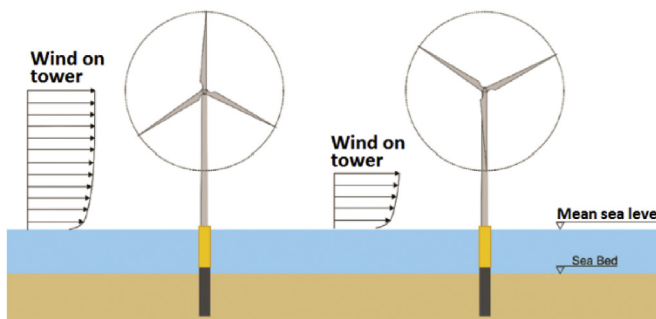


Fig. 2. Cyclic/dynamic load acting on the tower due to blade shadowing effect (3P load).

tower causing additional cyclic load on the structure at the frequency equal to $1P \times$ number of blades. Thus, 3P is the blade passing frequency for a three-bladed WT. Considering all the frequency contents of the applied loads, to design the support structure of WT, the design engineer targets support structure frequency range (i.e. the global frequency of the overall WT) which lies outside the frequency ranges of the rotor, blade passage of tower shade, wind and wave to avoid system resonance. Table 1 shows the 1P and 3P frequencies for some theoretical and commercial WTs.

In WT design, there are three possible intervals where the natural frequency of the support structure should lie. The frequency of the support structure should not fall into the 1P and 3P ranges. DNV guideline on design of offshore WT structures [27], stipulates that the natural frequency of WT lies in a narrow curve between the 1P and 3P frequencies which are specifically at least $\pm 10\%$ away from the 1P and 2P/3P frequencies. Under these design concepts, the frequency condition of the WT is said to be soft-stiff [20]. Fig. 3 shows typical allowable frequency range and excitation frequencies for commercial and reference WTs. The common choice for the frequency position of the support structures of present commercial WTs is in the *Soft-Stiff* region and this informed the use of test frequency that falls within soft-stiff in this research.

2.3. Service temperature of offshore wind turbine

Temperature is one of the most important extrinsic variables that influence the mechanical, fatigue and fracture behaviour of steels. Studies show that fatigue life reduces with increase in temperature [28]. However, the temperature effect on fatigue crack growth rate (FCGR) is rather not inconsequential and complex, and tends to have upper and lower limits [29]. The literature has shown that at free corrosion potential, a rise in seawater temperature from 5 °C to 20 °C doubled the rate of crack growth [28]. Substantial reduction in fracture toughness is seen at low temperatures, which reduces the critical sizes at fracture [29]. To eliminate ambiguities in corrosion-fatigue test results and to compare the results with published data, a range of temperatures pertinent to an offshore environment was maintained. The reported range for some of the offshore WTs are shown in Table 2. If reliability in the use of steel in the marine environment is of immense concern, then effect of temperature is evaluated in every case especially for OWT support structures. A map of the monthly sea surface temperature fluctuations around the UK shows an annual temperature range of 6–18 °C in January and August, respectively [30].

3. Steel materials for wind turbine support structures

The magnitude of stresses acting on WT is of primary concern to the design engineer because they directly determine the functionality and lifespan of the WT. Some of the many grades of structural steel which are widely used in fabrication of engineering components and structures across Europe are S195, S235, S275, S355, S420, and S460. Grades S235, S275, S355 are the common structural steel grades in use across EU for many construction projects [33]. Traditionally, European Standard EN10025 S355 (or EN 10225 S355) is the main structural steel typically in use in the design of WT structure [34,35]. The S355 steel subgrades which are given in this standard for design of offshore structures are shown in Table 3. The BS4360:1990 code in Table 3 has been withdrawn and replaced with EN10025 S355. In this table, “S” denotes structural steel and the sub-grade JR, J0, J2, K2 refers to material toughness at a particular temperature using Longitudinal Charpy V-notch impacts test methodology with “J” denoting notch impact test (performed at; JR: room temp, J0: 0 °C; J2: -20 °C). The simple meaning is that S355JR can withstand an impact energy of 27 J at 20 °C, S355J0 can withstand an impact energy of 27 J at 0 °C, S355J2 can withstand an impact energy of 27 J at -20 °C [35]. S355 N has impact energy of 40 J at -20 °C while S355NL has impact energy of 27 J at -50 °C [35]. N & NL denote normalised and normalised rolled weldable fine grain structural steels, respectively. The impact strength reduces as temperature decreases due to the fact that the steel becomes brittle. Therefore, if the structure is likely to experience temperatures as low as -20 °C, the appropriate choice of steel would be S355J2 rather than S355JR or S355J0.

As seen in Table 3, the minimum yield stress for S355 structural steel is 355 MPa which denotes the origin of the steel's name. However, the value of the yield strength decreases with increase in plate thickness as seen in Table 3. The Ultimate Tensile Strength (UTS) for S355 steel is between 470 and 630 MPa for thicknesses of up to 100 mm [38–41]. The general chemical composition of S355 is given in EN10025 and ASTM 572 standards and summarized in Table 4. Table 4 shows that S355 steel is generally a low carbon steel whose specifications offer ‘high’ yield strength and the value varies with the steel grade. Limited grades contain also the compositions that are in bold. Different sub-grades of S355 are selected for use in offshore applications which are often the M series grade. S355 M and S355ML are referred to as Thermo-mechanically rolled weldable fine grain structural steels where M stands for

Table 1
1P and 3P frequencies for some operational and reference offshore WTs.

Name	Rotor Freq. Range (1P) [Hz]	Blade passing Freq. Range (3P) [Hz]	Ref.
Vestas V66 2 MW turbine	0.18–0.41	0.54–1.23	[20]
Vestas V90 3 MW turbine	0.14–0.31	0.42–0.90	[20]
Siemens SWT-3.6 (MW)-107	0.08–0.22	0.24–0.66	[20]
Vestas V120 4.5 MW	0.17–0.25	0.50–0.75	[24,25]
NREL 5 MW WT	0.12–0.20	0.35–0.60	[19]
DTU 10 MW RWT	0.10–0.16	0.30–0.48	[10]
3 MW Sinovel WT	0.14–0.32	0.41–0.95	[17]

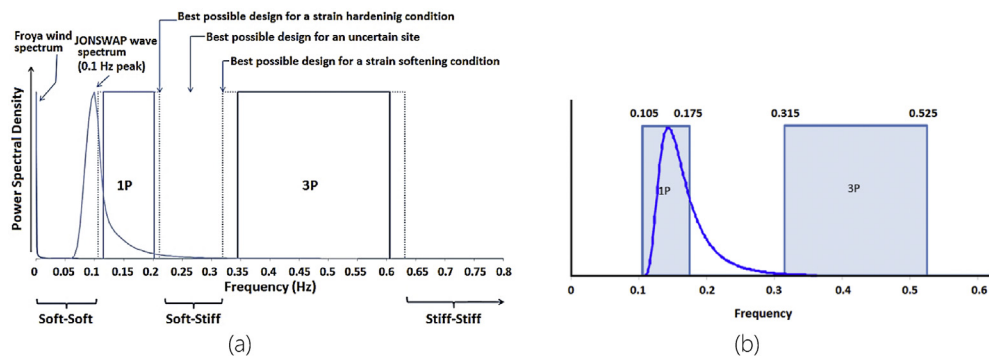


Fig. 3. The 1P and 3P frequency range for WTs. (a) for a 3 bladed NREL standard 5 MW wind turbine [19] (b) for the LEANWIND 8 MW reference turbine [26].

Table 2

Service temperature for some commercial WT.

Name	Operational Temperature range	Extreme Temperature range	Ref.
Vestas V164-8 MW turbine	–10 to 25 °C	–15 to 35 °C	[31]
SeaTitan 10 MW	–10 to 40 °C	–20 to 50 °C	[11]
Sway ST10	–10 to 30 °C	–20 to +40 °C	[32]

Table 3

Common structural steel grades for offshore design [34–37].

Non-alloy structural steels				
European	British	Minimum yield strength in MPa at thickness t (mm)		
EN10025 Part 2: 2004	BS4360:1990	3 ≤ t ≤ 16	16 < t ≤ 40	40 < t ≤ 63
S355 JR	50B	355	345	335
S355 JO	50C	355	345	335
S335 J2	–	355	345	335
S355J2+N	50D	355	345	335
S355 K2	50EE	355	345	335
S355K2+N	50DD	355	345	335
S355 N	50	355	345	335
S355NL	50EE	355	345	335
S355 M	–	355	345	335
S355ML		355	345	335

Table 4

General composition wt% (max) EN10025 S355 [ASTM 572] [37–44].

Present study	C	Mn	Si	Cu	N	P	S	Cr	Ni	Mo	V	Al	Fe
	0.22	1.60	0.55	0.55	0.02	0.06	0.035	0.03	0.50	0.10	0.12	0.02(min)	Bal

Thermo-Mechanical control rolled/(or process) (TMCR or TMCP).

Some advanced M series grades regarded as the modern material choice for XL wind turbine design [42] are shown in Table 5. These steel grades have been manufactured specifically for offshore pipelines, platforms, pressure vessels, and modern WT installations [42]. The material is essentially a very low carbon C-Mn steel. This steel exhibits very low Sulphur and Phosphorus content with an increase in Ni. Moreover, the alloying elements Si, Cu, Mo, N, and V are reduced making the material highly ductile. In addition, hot rolling gives the material a fine-grained microstructure.

The corrosion-fatigue resistance of mild steel in seawater has been found to degrade with dissolution of oxygen in the steel [43]. Generally, the advanced TMCP steels are vacuum degassed, fully killed and control rolled. Fully killed is achieved by the addition of some alloying elements to completely deoxidize or remove oxygen from the steel melt before casting. This prevents release of gases during solidification and hence eliminates gas porosity in the product. This practice gives the steel high degree of chemical homogeneity.

In general, the grading system of S355 follows the kind of heat treatment and/or thermo-mechanical processing given to the steel. It is extremely important that these steels are correctly specified, covering the strength grade and the steel sub-grade, in order to

Table 5

Mechanical properties of advanced M series S355 steel subgrades for XL offshore WT design Offshore Structural Steel Plates.

European	British	Typical application Min. yield strength R_{eH} (MPa) for thickness t (mm)					
Plates & tubulars							
EN10225	BS7191	t ≤ 25	25 < t ≤ 40	40 < t ≤ 63	63 < t ≤ 100	100 < t 150	Typical application
S355G7 + N	355EM	355	345	335	325	320	Primary Structure
S355G7 + M	355EM	355	345	335	325		Primary Structure
S355G8 + N	355EMZ	355	345	335	325		Critical Joints
S355G8 + M	355EMZ	355	345	335	325	320	Critical Joints
S355G9 + N		355	345	335	325	320	Primary Structure
S355G9 + M		355	345	335	325		Primary Structure
S355G10 + N		355	345	335	325	320	Critical Joints
S355G10 + M		355	345	335	325		Critical Joints

Tensile properties: R_m t(mm) ≤ 100 mm: 470–630 MPa; t(mm) > 100 mm: 460–620 MPa. Minimum elongation = 22%, Minimum average longitudinal Charpy V-notch impact test value = 50 J at -40°, for all the sub-grade. Max CEV: 0.41 or 0.42.

avoid brittle failure [36]. In other words, the intention of the structural classification is to serve as a guide in selecting the appropriate steel and suitable inspection to avoid brittle fracture.

As noted previously, TMCP steel is generally used for WT components shown in Fig. 1 and auxiliary attachments. For the completion of the Gemini Offshore Windfarm, Dillinger supplied approximately 94,500 tonnes of S355G8 + M plates with thicknesses of up to 95 mm for the farm steel foundations [16]. The currently estimated cost per tonne of some sub-grades of S355 steel is given in Table 6. Therefore, this implies that 94,500 tonnes of S355G8 + M steel plates supplied for the Gemini windpark would be valued at approximately £56.7 million. Thus, an informed and accurate steel selection has the capacity of saving millions of pounds for offshore windfarm construction.

LCOE is crucial to determine the viability of a windfarm. A key parameter in calculating LCOE is the lifespan of a wind turbine, where a greater lifespan results in lower LCOE (£/MWh). The lifespan can be estimated by prediction of corrosion-fatigue life and therefore maximum energy cost reduction can be achieved by the use of efficient and economic corrosion-fatigue resistant materials.

Presently, there are little or no public data available on corrosion-fatigue performance of advanced sub-grades of S355 steel. Thus, this experimental research seeks to examine how S355G10 + M steel grade compares with other grades in terms of tolerance for defects, and defect growth rate under the influence of fatigue and corrosion conditions, similar to an offshore environment. The information will be vital in:

- economic selection of advanced XL steel plates for the design of modern WT,
- prediction of operating lifetime of modern offshore WT with defects,
- provision of guidance on inspection requirements.

4. Experimental procedures

4.1. Test material and specimen

The corrosion-fatigue crack growth test material used in this study is a 90-mm thick plate of EN-10225:01 S355G10 + M steel, with inspection certificate of 3.2 as per EN 10204:2004. The subgrade is also known as 1.8813 + M. This steel is essentially a C-Mn steel, reported to have enhanced through-thickness ductility and impact energy verified at -40 °C. The material was reported by the manufacturer to have a Yield Strength, R_p (σ_y) of 460 MPa and Ultimate Tensile Strength, R_m (σ_{UTS}) of 561 MPa. A confirmatory tensile test performed prior to experiment gave Yield strength, R_p (σ_y) = 435 MPa, Tensile strength R_m = 545 MPa and tensile strain at failure of 38%. The values quoted is the average value of the two tests performed. The chemical composition of the steel subgrade is given in Table 7.

Compact tension, C(T), specimens were extracted from plate of 90 mm thickness, Fig. 4(a) and with dimensions as shown in Fig. 4(b), according to ASTM E647-15 standard [45]. The crack plane and direction of propagation are perpendicular to the rolling direction as schematically shown in Fig. 4(c). This orientation is the through-thickness and the most likely plane of crack initiation and propagation for monopiles. The test specimens were pre-cracked in air using force shedding (or K-decreasing) method as described in Ref. [45]. The pre-crack length for a given machined V-notch was at least 1.5 mm and no more than 3.5 mm. The load ratio

Table 6

Cost of Wind Turbine steel as at September 2017.

S355 steel grade	£/tonne
EN10025: S355JR, S355J0, S355J2	£303 - 380
EN10025: S355JR, S355J0, S355J2 with normalization.	£349 - £644
EN10025: S355G8 + M, S355G10 + M – TMCP steels	£600-680

Table 7

The chemical composition in weight percent of S355G10 + M.

C	Mn	Ni	Si	Cu	Cr	NB	P	Mo	N	Ti	V	S	Fe
0.06	1.57	0.334	0.271	0.241	0.034	0.022	0.013	0.006	0.004	0.003	0.001	0.001	Bal

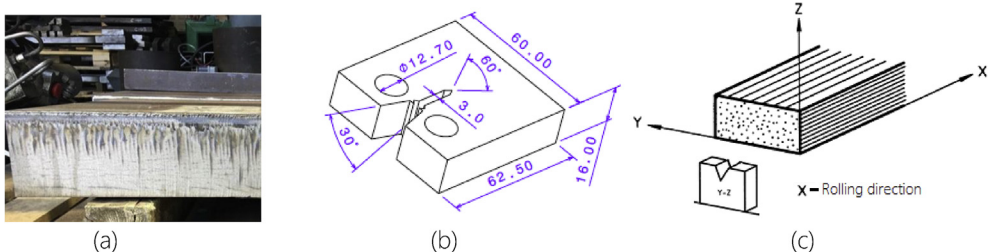


Fig. 4. Test material and specimen. (a) 90 mm S355G10 + M thick plate, (b) C(T) specimen in accordance with ASTM E647 –15 [45], (c) Orientation of the crack plane.

for pre-cracking was 0.1 and loading frequency of 4 or 5 Hz.

4.2. Test set-up and environment

Instron 8801 fatigue test rig as shown in Fig. 5(a) was used to perform the fatigue crack growth test. It is a servo-hydraulic machine of 100 kN frame capacity, with modern digital controllers, set-up in accordance with the standards enumerated in Ref. [46]. The machine has an actuator stroke of \pm 75 mm. Air tests were conducted at laboratory ambient temperature conditions of approximately 20 °C.

As concentrations of ocean water vary with sampling location, consistency was maintained with the literature through the use of substitute seawater in accordance with ASTM D1141-98. The composition of the artificial seawater is given in Table 8 [47].

Before the start of corrosion-fatigue tests, pre-cracked specimens were soaked in seawater for 2 days. The specimen was then fixed to the grips of the fatigue testing machine. The seawater was circulated using pumps past the C(T) specimen in a Perpex chamber as shown in Fig. 5(c), at a continuous rate of 4L/min. During the test, the temperature of the seawater in the chamber was controlled using Hailea refrigeration unit, Fig. 5(d), and varied between 7.5 °C to 8.2 °C. The pH level at the beginning of the experiment was

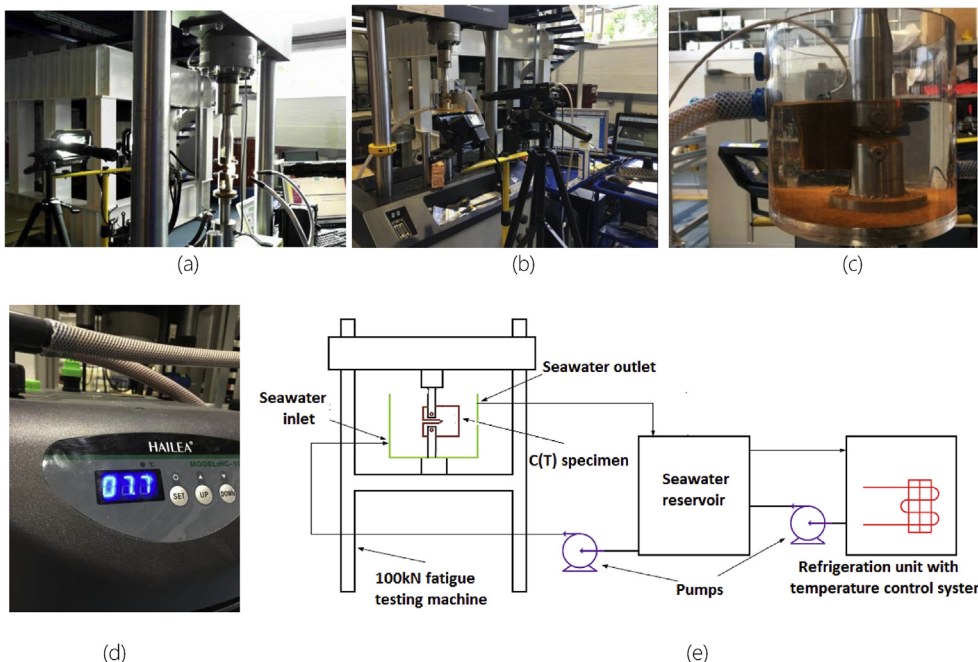


Fig. 5. Corrosion fatigue setup for the present study. (a) Fatigue test set-up in air, (b) Fatigue test set-up in seawater, (c) Seawater chamber with test specimen, (d) Hailea Chiller for temperature control, and (e) Schematic representation of complete fatigue testing circuit.

Table 8
Chemical composition of substitute seawater water [47].

Compound	Concentration, g/L
NaCl	24.53
MgCl ₂	5.20
Na ₂ SO ₄	4.09
CaCl ₂	1.16
KCl	0.695
NaHCO ₃	0.201
KBr	0.101
H ₃ BO ₃	0.027
SrCl ₂	0.025
NaF	0.003

8.1, which decreased with time until a level of pH 7.7 where the seawater was subsequently replaced. In total, 70 L of seawater was used for each experimental run where the specimen was completely immersed in the seawater throughout the test period. Fig. 5(e) shows the complete experimental set-up for this study.

4.3. Loading conditions for laboratory based experiments

The materials evaluation for structural integrity assessment of offshore wind monopiles starts by considering the effects of WT operational frequency, wind loading waveform and mean stress on the fatigue crack growth rate (FCGR) of the structural steel in air and seawater. In many fatigue tests, the waveform that is usually employed is sinusoidal wave of constant cyclic loading amplitude [48] and a constant mean load. For this paper, the corrosion-fatigue crack growth rate (CFCGR) and comparisons with recent studies under sinusoidal wave of constant cyclic loading amplitude is presented. Study is on-going to determine the effect of waveforms on the CFCGR of S355 steel under conditions pertinent to WT operational environment. Tests were conducted in air and in free-corrosion (no cathodic protection) conditions using constant amplitude sinusoidal waveform as shown in Fig. 6, at load ratio R = 0.1 and loading frequencies of 4 Hz and 5 Hz in air, and at 0.3 Hz in the substituted seawater. Fig. 6(a) shows the representation of constant amplitude stress vs. time curve with main test parameters for the fatigue crack growth (FCG) tests. Fig. 6(b) presents the 0.3 Hz waveform used for the present study and Fig. 6(c) shows the unipolar phase angle of the experimental sinewave.

Tests were conducted under load control mode. Before commencing the experiments, the machine load cells were calibrated dynamically as recommended in BS Standard [49] to a level of 1.5 times the maximum test load. The machine grips were accurately aligned using the double pin-clevis arrangement. The fatigue and corrosion fatigue tests complied with the literature [45,50]. To take readings, the waveform was held at the P_{max} for 30 s. This interruption of cyclic loading to take readings is permissible [45] as long as care is exercised to avoid introducing transient crack extension or growth under static force requiring a hold period of less than 10 min. The frequency used for seawater environment was determined by considering the operational frequency of commercial WTs in the soft-stiff (0.18–0.315 Hz) region as shown in Fig. 3. Previous literature used 0.3 Hz for corrosion-fatigue studies of monopile steels [46,48] and therefore in this paper, tests in seawater were performed with the same frequency. Note that fatigue crack growth rate (FCGR) in air is found to be approximately constant in the range 0.1 Hz and 5Hz [51], whereas FCGR is sensitive to cyclic frequency in seawater environment.

4.4. Crack length measurement

Crack lengths were measured in air using digital cameras and in some cases travelling microscope. For seawater test, the presence of an environmental chamber containing an aqueous solution hides the crack tip, necessitating the use of a nonvisual technique as recommended in Ref. [45]. Hence, in seawater the Back-Face Strain (BFS) method was used. BFS is shown to be highly reliable in

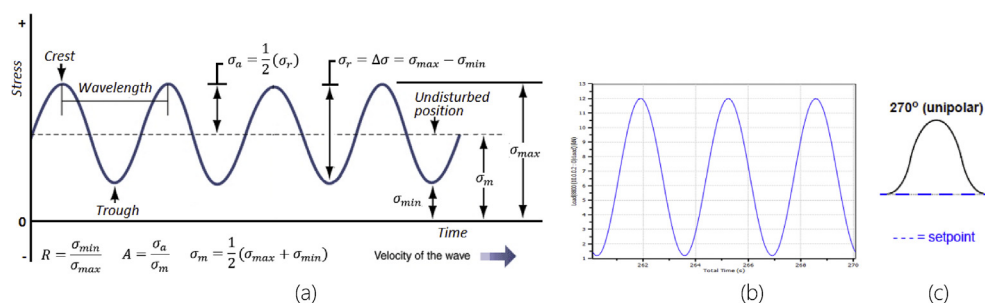


Fig. 6. Sinusoidal waveform. (a) Constant amplitude cyclic loading vs. time curve, (b) 0.3 Hz sine waveform for the present study and (c) 270°-unipolar phase angle.

measuring crack growth in seawater more than Alternating Current Potential Difference (ACPD), Direct current potential difference (DCPD) and optical measurements [48]. It is simple and cost effective, but thorough understanding on how it is used is needed, because minor error in strain gauge installation could lead to large error in crack growth measurement [52]. To use the BFS method in measuring crack length in seawater, calibration correlating the crack length in air with amount of microstrain was made. Fig. 7(a-d) shows measurement of crack length in air using StreamPix5 digital cameras on both sides of the C(T) specimen. In some occasions, travelling microscope was used to check side differences. If at any point the difference between the crack length at front and back differed by 2 mm, the test was terminated. Throughout the tests, the difference in the crack length for the two faces was less than 2 mm. This is because, it was always ensured that the C(T) specimen was accurately aligned perpendicularly to the loading axis and specimen centralized within grips.

To measure the microstrain, Linear Electrical Resistance Strain Gauges were installed at the back face of the C(T) specimens. Fig. 7(e) shows an installed strain gauge at the back of the C(T) specimen and the installation complied with instructions as given in Refs. [53–55]. The lead wires were soldered to the strain gauge through the connecting tabs in accordance with [56], and the other ends of the wires connected to a Vishay P3 microstrain indicator and recorder, Fig. 7(f).

Gauge factor balancing and overall operation of the strain box can be found in Refs. [57] and [58]. After seawater test, the crack morphology, specifically crack branching or out-of-plane cracking which may render the test invalid as per ASTM E647-15 used in this programme was checked, see Fig. 7(g).

Before setting C(T) specimen into the fatigue machine's grips, its surface was polished with 320 and 400 grit abrasive papers and using indirect lighting to aid in the resolution of the crack tip in air test. During the air tests, the elapsed cycles, N, crack length, a and microstrain, ϵ values were recorded. The average value of the crack lengths measured on the two faces was taken as the mean crack length and used in the calculations. The calibration curves that correlate the crack length with the microstrain given by the strain gauge for P_{max} of 12 kN, 10 kN and 9 kN obtained for seawater measurement are shown in Fig. 8.

It can be seen from Fig. 8 that BFS calibration function depends on the loading conditions. This implies that varying load levels require development of different calibration function. It is important to always quote the strain gauge used for calibration. In this test, it was observed that using different linear strain gauges for calibration could cause significant variation in the BFS curve. This underscores the need for consistency in the use of same strain gauge type for a given corrosion fatigue study. Fig. 8(b) shows the strain gauge used for this study - CEA-06-240UZ-120 gauge of Vishay Precision Group, having gauge factor of 2.14, grid resistance 120 \pm 0.3% and gauge length of 6 mm. It works well in the temperature range of (-75° to $+175^{\circ}$ C) [49].

The strain gauge on the C(T) sample for seawater test was protected against the corrosive environment by coating with M-Coat JA [59]. It is a two-part polysulfide, liquid polymer compound, that when mixed and fully cured forms a rubber-like covering that provides an effective barrier against the seawater and also protects the installations from mechanical damage. The initial conditions of the C(T) specimens before start of test are given in Table 9 and all length measurements are in mm. As seen in this table, a total of 10 tests were conducted: 5 were performed in free-corrosion seawater environment at frequency of 0.3 Hz and the rest were tested in

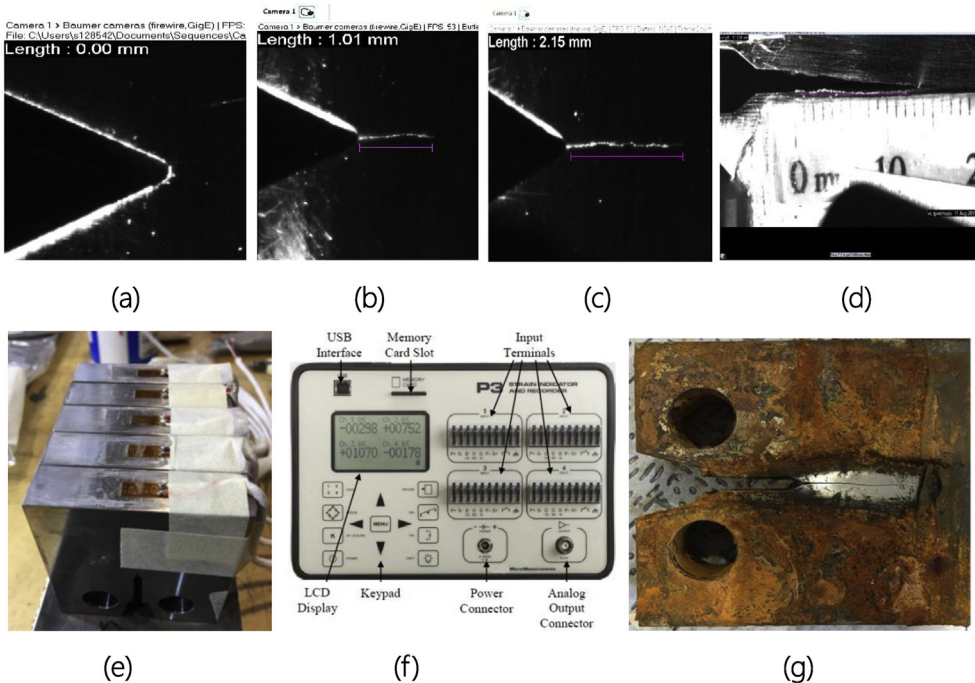


Fig. 7. Fatigue crack length measurement. (a-d) measurement using StreamPix5 digital cameras in air, (e) strain gauge bonded to C(T) samples, (f) front panel view of microstrain gauge reader, (g) examination of tested sample.

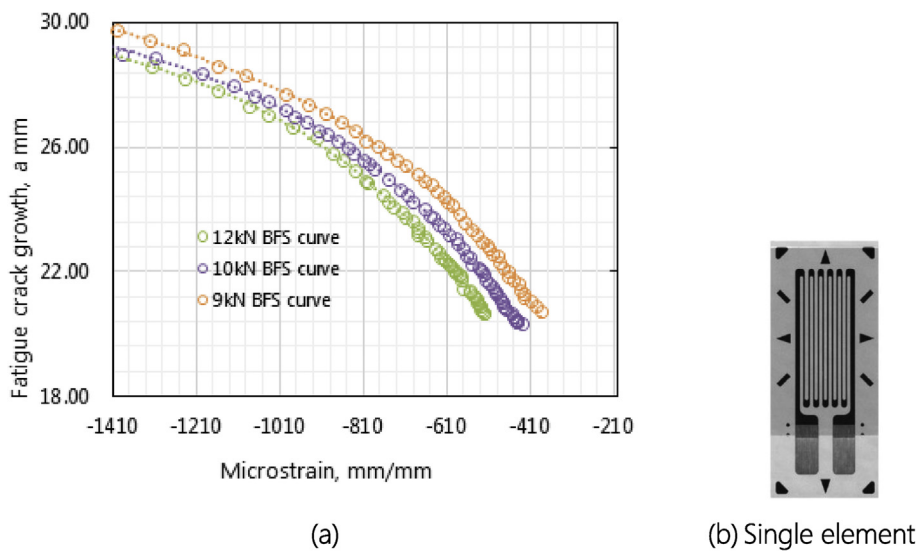


Fig. 8. Empirical Back-Face Strain (BFS) curves. (a) crack length correlation curves for the present study, (b) Single element strain gauge.

Table 9
Test specimen dimensions (mm) and loading conditions at $R = 0.1$

Test No.	Environment	W	B	a_0	a_f	f (Hz)	P_{max} (kN)
AS12	Air	50.00	16.00	24.86	32.46	4	12
AS10a	Air	50.01	16.00	20.30	29.53	5	10
AS10b	Air	50.00	16.00	24.75	32.81	4	10
AS9	Air	50.00	16.03	20.74	30.95	5	9
AS8	Air	50.15	16.00	24.39	33.65	5	8
SS12	Seawater	50.00	16.00	25.33	31.18	0.3	12
SS10a	Seawater	50.03	16.05	20.34	29.41	0.3	10
SS10b	Seawater	50.03	16.04	20.80	29.61	0.5	10
SS9a	Seawater	50.01	16.16	21.69	29.30	0.3	9
SS9b	Seawater	50.05	16.06	21.95	30.21	0.5	9

air.

4.5. Fatigue crack growth rate calculation

The LEFM approach was used in the calculation of crack propagation rates, where the values of N , a and $\mu\epsilon$ were measured of the strain gauge in air. For seawater test, N and $\mu\epsilon$ were obtained throughout the test. Using the appropriate calibration curve (Fig. 8), the $\mu\epsilon$ was converted to crack length and subsequently the CFCGR rate, da/dN (crack increment per cycle) vs. ΔK (stress intensity factor range (SIFR)) was plotted on a log-log graph. The da/dN was calculated using seven-point incremental polynomial method as described in Ref. [45]. The LEFM ΔK was calculated using the equation [45,50]:

$$\Delta K = \frac{\Delta P}{(B\sqrt{W})} \times \frac{(2 + \alpha)}{(1 - \alpha)^{1.5}} \times \left(0.886 + 4.64\alpha - 13.32\alpha^2 + 14.72\alpha^3 - 5.6\alpha^4 \right) \quad (1)$$

where ΔP is the applied cyclic load range, B is the specimen thickness, W is the width of the specimen, a is the crack length and $\alpha = a/W$. The damage-tolerant design approach of structures assumes that every structural member contains flaws in the form of cracks. Above a certain critical combination of nominal stress range and crack length (or ΔK), commonly referred to as the threshold, ΔK_{th} , the existing crack in the material grows. Region II, which is usually the linear part (in log-log axes), is generally used for design purposes. This paper focuses on region II, and the equation describing this region is commonly referred to as the Paris Law. The Paris law is obtained from a straight line drawn through the linear part of the curve and given as:

$$\frac{da}{dN} = C\Delta K^m \quad (2)$$

where C and m are empirical power-law constants found by fitting a regression line to the test data. It is pertinent to note that fatigue test, especially corrosion-fatigue test, has significant level of data scatter. Hence, in design a factor above the mean value is commonly used. This paper only compares the mean value of the fatigue data generated.

5. Experimental results and discussion

5.1. Air tests

In all the tests and comparative analysis in this paper, the units m/cycle for da/dN and MPa/m for SIFR were used. The experimental results obtained for FCGR tests in air in the present study (PS) are shown in Fig. 9. The result shows that in the Paris region, mean stress and frequency have little or no effect on the FCGR in S355G10 + M steel in air within the range of frequencies considered. An interesting observation is that, regardless of the starting crack length within the range used in this programme or ΔK , similar curve trends were obtained in the Paris region. It is also observed that threshold convergence appears to be dependent on the initial stress intensity factor range (SIFR) or crack length.

In Fig. 9 (a), 10 kN air test was performed twice using different frequencies and the result shows a similar trend in the Paris region. A mean curve is fitted to the air test results by removing the threshold converging points, and treating the whole linear or Paris-region data points as if they were obtained from one test. The non-linear data removed are those below 19.13 MPa/m for 10 kN, 5 Hz; 27.48 MPa/m for 10 kN, 4 Hz; and 17.11 MPa/m for 9 kN. Note that the whole data points are presented in Fig. 9 (a) with the mean line from linear data points inserted. Using simplified Paris-law and shape function solutions as contained in ASTM E647 [45] and BS ISO 12108: 2012 [60], the mean curve is defined by the equation $da/dN = 1.01 \times 10^{-13} \Delta K^{4.12}$ while the power law equation for the mean plus 2 standard deviation (mean + 2SD) in air is obtained as $da/dN = 1.66 \times 10^{-13} \Delta K^{4.12}$.

In Fig. 9 (b) the result of the present study is compared with SLIC joint industry projects' [46,61] fatigue data for S355G8 + M in air. The C(T) specimen for SLIC project was machined from 90-mm thick EN-10225:01 S355G8 + M steel plate, with inspection certificate of 3.2 as per EN 10204:2004 and certified by Germanischer Lloyd. The chemical composition of the steel subgrade is given in Table 10.

With regards to the composition, S355G8 + M and S355G10 + M are fundamentally the same. The SLIC mean plus 2SD curve for air test data is described by the equation $da/dN = 3.54 \times 10^{-12} \Delta K^{3.3}$ and this curve is re-produced in Fig. 9(b) while the SLIC mean curve equation for the air data is given as $da/dN = 2.83 \times 10^{-12} \Delta K^{3.23}$. Notice that SLIC tests were done at different test centres for the same loading condition, 10 kN, 2 Hz. It can be seen that the FCG gradient in the present study on S355G10 + M is more inclined and showing more resistance to FGC than the SLIC S355G8 + M especially at low SIFR. At higher values of SIFR, the crack growth rates for the two subgrades appear to converge and fall close to each other. Studies have shown that little scatter is observed for FCGR of steel in air. Considering this, the SLIC mean + 2SD curve appears to capture the upper scatter bound for the S355 TMCP steels. BS7910:2013 + A1:2015 recommended designing steel structures using FCGR of $\frac{da}{dN} = 1.65 \times 10^{-11} \Delta K^3$ in air for steels with yield strengths less than 700 MPa. This curve has been reproduced in Fig. 9 (b). It is obvious that the design curve is much more conservative for the air data.

An interesting study on S355 steel was carried out by Thorpe et al. [28]. The authors investigated the fatigue crack growth (FCG) properties of steel manufactured to BS4360 Grade 50D steel in air. This steel is equivalent to BS4360:1990 S355J2 + N. The C(T) specimen was extracted from 38 mm thick plate, with the composition of this steel given in Table 10. The quoted mechanical properties of the steel are: $\sigma_y = 370$ MPa, $\sigma_{UTS} = 538$ MPa, Elongation (%) = 32.

The test was performed in laboratory air conditions with frequency varying from 1 to 0.85 Hz. The result from this work stated that the stress ratio, R, had little or no effect on FCGR in air and that FCGR in air does not depend on the specimen thickness. The 2-

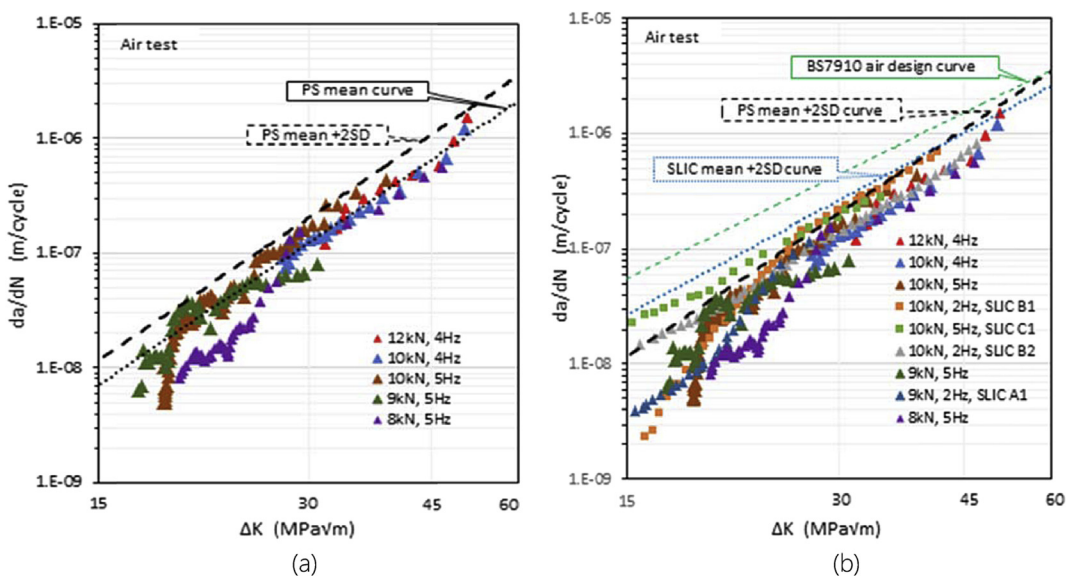


Fig. 9. FCGR in air (a) for S355G10 + M in the present study (b) Comparison of S355G10 + M with S355G8 + M in the SLIC study.

Table 10

Composition (wt%) of S355 steels used in this study.

Steel	C	Mn	Ni	Si	Cu	Cr	NB	P	Mo	N	Ti	V	S	Al	Fe
Present study	0.06	1.57	0.33	0.27	0.24	0.034	0.022	0.013	0.006	0.004	0.003	0.001	0.001	–	Bal
SLIC	0.053	1.52	0.32	0.27	0.24	0.028	0.020	0.012	0.007	0.004	0.001	0.001	0.001	–	Bal
Scott	0.18	1.38	–	0.37	–	–	0.034	0.032	–	–	–	0.01	0.024	–	Bal
Thorpe	0.17	1.35	0.07	0.35	0.17	0.09	0.03	0.037	0.01	–	0.01	0.01	0.023	0.05	Bal
Jesus	0.10	0.64	0.10	0.15	0.38	0.08	–	0.022	0.014	–	–	0.003	0.041	–	Bal
Dhinakaran	0.09	1.45	0.072	0.38	–	0.07	–	0.004	–	–	–	–	0.004	–	Bal
Tsay	0.13	1.32	0.03	0.31	–	0.03	–	0.02	–	–	–	–	0.01	–	Bal

stage curve, as recommended in Ref. [62], was defined using the mean curve line. Their FCGR for Stage A was given as $da/dN = 3.26 \times 10^{-12} \Delta K^{3.27}$, while that of Stage B was $da/dN = 2.44 \times 10^{-11} \Delta K^{2.67}$ as shown in Fig. 10.

Scott et al., in 1983 [63] also studied S355J2+N (BS4360 Grade 50D) steel. The C(T) for this experiment had thickness of 37.5 mm extracted from the steel plate in the L-T (Longitudinal-Transverse) orientation. The plate was hot-rolled and normalized, with composition as shown in Table 10. Table 10 assumes that the C(T) was extracted from 76 mm plate. The quoted mechanical properties of the steel are: $\sigma_y = 360$ MPa, $\sigma_{UTS} = 545$ MPa, Elongation (%) = 26 and Charpy impact value (J) at $-30^\circ\text{C} = 117$. The test was performed in laboratory air condition. In Scott's work [63], cyclic frequency and stress ratio (in the range 0.85–1.0) had little or no influence on the FCGR in air. 2-stage Paris-law trends was used to describe the FCGR of the whole test in air. The FCGR for Stage A is given as $da/dN = 5.89 \times 10^{-12} \Delta K^{3.15}$, while that of Stage B is $da/dN = 2.80 \times 10^{-11} \Delta K^{2.65}$. The FCGRs are essentially the same to that of Thorpe et al. and so not reproduced.

Jesus et al. [64] also studied fatigue growth in S355 steel. The subgrade name and the production history were not stated. The mechanical properties of the actual steel studied was quoted to be $\sigma_y = 419$ MPa and $\sigma_{UTS} = 732$ MPa. It should be noted that tensile property of S355 is usually given in yield stress range of 470–630 MPa for t (mm) ≤ 100 mm and 460–620 MPa for t (mm) > 100 mm. The chemical composition of the material is shown in Table 10. Using a C(T) specimen manufactured to ASTM E647 standard, FCG test was performed. Four stress ratios were used by de Jesus et al.: 0, 0.25, 0.5 and 0.75. The crack growth was measured using a magnifying device with resolution of 1 μm . The frequency of test was reported to be 20 Hz, which was reduced at region of high FCGR, taken to represent approximately 0.3 mm per 1000 cycles. The results show that the stress ratios again have no effect on the FCGR in air. However, the authors noted that there was crack closure effect for tests performed at about zero stress ratios and this reduced the effective SIFR applied, hence a reduced FCGR was obtained as was verified experimentally. The crack closure effect reduces with increase in R , so that the applied SIFR was fully effective. Fig. 10 shows the mean air Paris curve for the study. The FCGR was given as $8.58 \times 10^{-13} \Delta K^{3.74}$ where da/dN is in m/cycle and ΔK in MPa $\sqrt{\text{m}}$.

Tsay [65] studied the FGCR of a marine EH36 steel whose composition is also shown in Table 10 and the yield strength given as 420 MPa. The steel was thermo-mechanically-control processed, commonly specified as fine-grained high tensile steel and generally used in the design of ship bodies. For normalized condition, the nearest equivalent of this steel is S355J2+N. The test result selected in this analysis was the crack growth direction normal to the rolling direction (LT specimen). The result of the FGR test is also

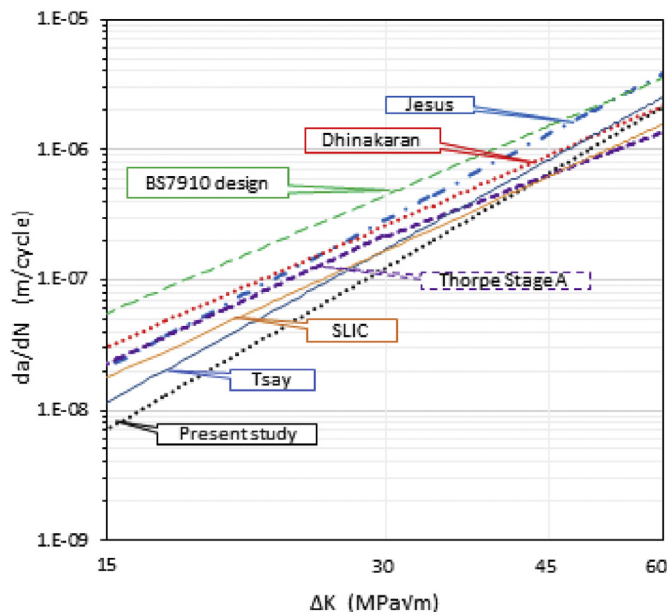


Fig. 10. Comparison of FCGR in air for S355 steel subgrades.

included in Fig. 10.

A standard C(T) manufactured as per ASTM E647 was used by Dhinakaran and Prakash [51] to study the corrosion-fatigue property of a steel with a composition as shown in Table 10. The subgrade name was not given. The mechanical property of the steel is given as $\sigma_y = 459$ MPa, $\sigma_{UTS} = 530$ MPa and elongation 33%. The test, performed under constant frequency amplitude and at constant SIFR is also included in Fig. 10. The mean FCGR power law constants for various S355 grades considered in this study are shown in Table 11. The table shows increase in the Paris exponent in the TMCP steels, which implies that the TMCP curves are more inclined.

In general, this study shows that S355 TMCP steels offer high fatigue damage tolerance than conventional S355 steels in air. In other words, FCGR is lowest in the TMCP steel compared with common steels studied. Reliable factor of difference between common and TMCP S355 steel will be established by considering more tests and this may be considered by the authors in future study. However it is clear that TMCP steels have superior resistance to fatigue crack propagation in air for S355 steel, and the factor decreases and tends to common value with increase in SIFR. Thus, in terms of structural application in air environment, where fatigue is the dominant issue selection of TMCP steels will be preferable. Fig. 10 also shows the inclusion of BS7910 curve (green curve) to the fatigue tests plots. It can be seen that the current BS7910 design curve in air is much more conservative for TMCP S355.

5.2. Seawater tests

The CFCGR results obtained for freely corroding conditions in seawater (SW) for the present study are shown in Fig. 11 (a). The mean curve is described by the equation $da/dN = 2.76 \times 10^{-12} \Delta K^{3.35}$ while the mean + 2SD curve is $da/dN = 5.49 \times 10^{-12} \Delta K^{3.35}$. The mean + 2SD satisfactorily enclosed all the data points in the Paris region.

Fig. 11(b) compares the CFCGR of the present study with the SLIC project study [46] on S355G8 + M. The SLIC tests were performed at different centres, thus tests under the same loading condition performed at different centres have been included. The CFCGR for the mean + 2SD curve, which serves as the upper scatter bound for the SLIC project is given as $\frac{da}{dN} = 1.25 \times 10^{-12} \Delta K^{3.86}$. What is apparent for the TMCP steels in Fig. 11(b) is that the difference in the mean load appears not to have a defined effect under the 0.3 Hz. Generally, if material variability is considered, it can be concluded that CFCGR in the two steel subgrades are the same at frequency of 0.3 Hz.

It is commonly observed that FCGR in seawater shows much greater scatter than that in air, especially at low SIFR. The SLIC mean + 2SD curve appears to closely represent the upper limit scatter bound for the S355 in seawater. For steel structures in marine environments with temperature up to 20 °C, with or without cathodic protection, BS7910:2013 + A1:2015 is recommended utilising the simplified Paris law $da/dN = 7.27 \times 10^{-11} \Delta K^{3.0}$ as the CFCGR, where da/dN has units m/cycle and ΔK is in MPa/m. The current BS7910:2013 + A1:2015 seawater upper bound design curve has been included in Fig. 11 (b). It can be seen that the current BS design curve for seawater is significantly conservative for the thick S355 TMCP steel.

Fig. 12 compares the S355 TMCP data presented in Fig. 11(b) with works of Thorpe, et al [28]. and Scott et al. [63]. It is pertinent to point out that Scott's SW test on S355J2 + N was performed at higher stress ratio $R = 0.5$, and lower frequency 0.1 Hz, temperature range 5–10 °C, and using triangular waveform at freely corroding potential (- 0.65 V). A sinewave of 0.1 Hz approximates to sea-wave frequency. The use of sea-wave frequency was an attempt to obtain fatigue data for application in offshore oil/gas production and exploration platforms. This would then enable extrapolation of the laboratory data to field structures. Severally tests have shown that triangular waveform test results are comparable to those obtained from the sinewave tests [63]. The Thorpe's test was performed using $R = 0-0.1$, sinewave and under free corroding condition.

As seen in Fig. 12, the data points obtained from different test programmes fall upon or close to each other with slight differences which can be attributed to inherent material variability. In general, the figure clearly shows that there is no difference in FCGR in SW for all the S355 ferritic steels. In order words, in terms of CFCGR, TMCP subgrades appear not to be superior to common or normalized S355 steels. Thus, in structural application in SW environment, where fatigue is the dominant issue, this study suggests that there is no justification for the market price difference between thick S355 TMCP and normalized S355. Table 12 lists the upper bound (mean + 2SD) FCGR power law constants in seawater for the present study, SLIC and that of BS7910 design curve in seawater.

Table 11
FCGR power law constants for various S355 grades considered in this study.

Study in air	FCGR (da/dN)
Present (TMCP)	$1.01 \times 10^{-13} \Delta K^{4.12}$
Tsay (TMCP)	$3.07 \times 10^{-13} \Delta K^{3.89}$
SLIC (TMCP)	$2.83 \times 10^{-12} \Delta K^{3.23}$
Jesus (Unknown)	$8.58 \times 10^{-13} \Delta K^{3.74}$
Thorpe* (Normalized)	$3.26 \times 10^{-12} \Delta K^{3.27}$
Scott* (Normalized)	$5.89 \times 10^{-12} \Delta K^{3.15}$
Dhinakaran (Unknown)	$7.56 \times 10^{-12} \Delta K^{3.07}$
BS7910 air design curve	$1.65 \times 10^{-11} \Delta K^{3.0}$

*Stage A only is included for Scott and Thorpe.

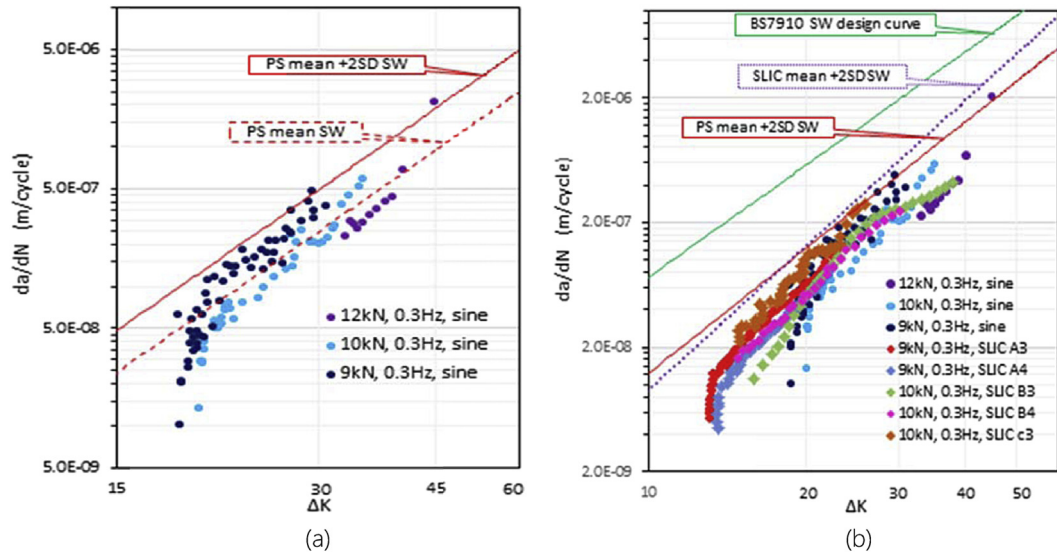


Fig. 11. CFCGR of S355 in seawater (SW) under free-corroding conditions. (a) CFCGR for S355G10 + M in SW (b) comparing CFCGR of S355G10 + M with SLIC study on S355G8 + M in SW.

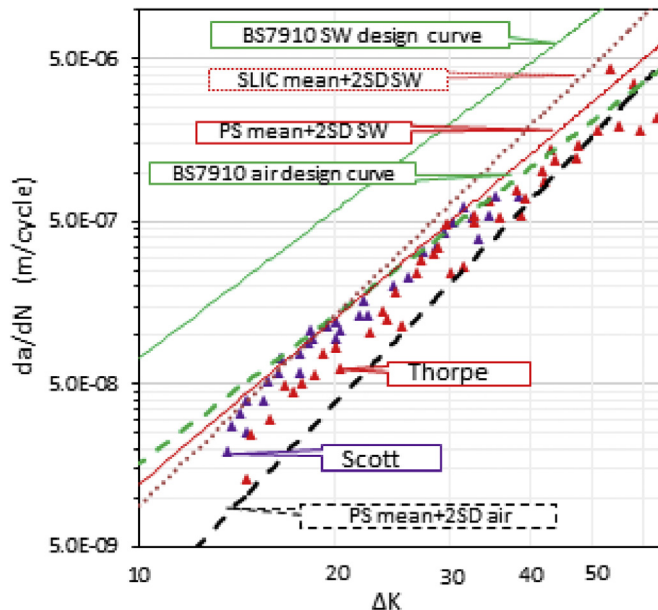


Fig. 12. CFCGR of S355 in seawater (SW) under free-corroding conditions.

Table 12
Upper bound FCGR power law constants in seawater.

Study in SW	FCGR (da/dN)
PS mean + 2SD	$5.49 \times 10^{-12} \Delta K^{3.35}$
SLIC mean + 2SD	$1.25 \times 10^{-12} \Delta K^{3.86}$
BS7910 SW design curve	$7.27 \times 10^{-11} \Delta K^{3.00}$

5.3. Environmental reduction factor (ERF)

Fig. 12 also shows the comparison of the mean + 2SD curves of the present study with current design curves in BS7910 for tests in air and SW. To explain the figure, the environmental reduction factor (ERF) at equal interval of ΔK for the present study is presented

Table 13

Environmental reduction factor (ERF) and Design conservative factor (DCF).

Present study (ERF)		BS7910 air DCF (PS)		BS7910 SW DCF (PS)		BS7910 SW DCF (SLIC)	
ΔK	ERF	ΔK	DCF-air	ΔK	DCF -SW	ΔK	DCF -SW
20	3.34	20	3.46	20	4.68	20	4.54
30	2.35	30	2.22	30	4.10	30	3.13
40	1.92	40	1.57	40	3.62	40	2.42
50	1.62	50	1.25	50	3.44	50	2.02
Average	2.31	Average	2.13	Average	3.96	Average	3.03

in Table 13. Design conservative factor (DCF) has been used here to make comparison with the BS7910 curves.

By analysing the crack growth rates in air and SW using the fitted mean + 2SD bounds in the SIFR 20–50 MPa \sqrt{m} , ERF is seen to decrease with increase in SIFR and an average reduction factor of 2.31 is obtained. In other words, the SW generally accelerated the FCGR by a factor of 2.31. The DCF between air test and BS7910 curve for fatigue design in air environment is 2.13. Since scatter in fatigue data in air is minimal compared to test in aggressive medium, the current BS7910 air curve satisfactorily and conservatively defines the upper FCGR bound for all the S355 steels. An average DCF of 3.96 for the present study and 3.03 for SLIC are obtained between SW test and BS7910 curves for design in seawater. It can be seen that the BS7910 curve in SW is much more conservative for the S355 steels considered. This increase in conservativeness will reduce the true lifespan of modern WT and impact unfavourably the LCOE.

6. Conclusions

This paper presents the FCGR performance of TMCP S355 steel in air and seawater, and compares the results with studies on common S355 steel sub-grades. The tests in this study were performed in accordance with BS 7910:2013 + A1:2015 and ASTM E647-15. Constant amplitude sinusoidal waveform was used at load ratio, R of 0.1 and loading frequencies of 4 Hz and 5 Hz in air, and at 0.3 Hz in artificial seawater. Air tests were performed at laboratory ambient temperature of approximately 20 °C, while the seawater environment temperature varied from 7.5 to 8.2 °C. Crack lengths were measured in air using digital cameras and in some cases travelling microscope. Back Face Strain (BFS) method was used to measure crack growth in seawater. The following conclusions have been drawn from this study:

1. The FCGR in advanced S355, particularly the subgrades S355G8 + M and S355G10 + M steels are essentially similar in seawater. However, S355G10 + M examined in this study generally shows more resistance to FCG in air compared to S355G8 + M particularly at lower values of SIFR.
2. The general upper bound Paris law describing the FCGR in thick S355G10 + M steel in air can be stated as $\frac{da}{dN} = 1.66 \times 10^{-13} \Delta K^{4.12}$ while that of seawater is found to be $\frac{da}{dN} = 5.49 \times 10^{-12} \Delta K^{3.35}$.
3. With respect to the mean + 2SD upper bound curves, the FCGR in S355G10 + M steel in seawater is higher than that of the air by an average factor of 2.31 throughout the Paris region in the range of ΔK: 20–50 MPa \sqrt{m} .
4. In general, this study shows that S355 TMCP steels offer high fatigue damage tolerance than normalized S355 steels in air and the factor decreases and tends to common value with increase in SIFR. In terms of structural application in air environment, where fatigue is the dominant issue selection of TMCP steels will be preferable.
5. Within the limit of test data analyzed, there is no difference in FCGR in SW for all the S355 ferritic steels. In order words, in terms of CFCGR, TMCP subgrades are not superior to normalized S355 steels. This suggests that a range of material choices are available for economic selection of S355 steel for wind farm support structure development.

Acknowledgements

This work was supported by grant EP/L016303/1 for Cranfield University and the University of Oxford, Centre for Doctoral Training in Renewable Energy Marine Structures - REMS (<http://www.rems-cdt.ac.uk/>) from the UK Engineering and Physical Sciences Research Council (EPSRC). Victor Igwemezie would like to acknowledge Tertiary Education Trust Fund (TETFund), Nigeria for financial support.

Appendix A. Supplementary data

Supplementary data related to this article can be found at <http://dx.doi.org/10.1016/j.marscr.2018.06.008>.

References

- [1] WindPower. The 10 biggest turbines in the world. 2016 Available at: <http://www.windpowermonthly.com/10-biggest-turbines>, Accessed date: 10 April 2016.
- [2] Caduff M, Huijbregts MAJ, Althaus HJ, Koehler A, Hellweg S. Wind power electricity: the bigger the turbine, the greener the electricity? Environ Sci Technol

- 2012;46(9):4725–33. <http://dx.doi.org/10.1021/es204108n>.
- [3] Kallehave D., Byrne BBW., LeBlanc Thilsted C., Mikkelsen KK., Association EWE., Estate TC., et al. Optimization of monopiles for offshore wind turbines. Philosophical transactions. Series A, Mathematical, physical, and engineering sciences. The Royal Society; 28 February 2015; 373(February 2015): 1–15. Available at: <http://dx.doi.org/10.1098/rsta.2014.0100> (Accessed: 29 July 2016).
- [4] OWPB. Cost reduction monitoring framework 2015. UK. 2015. p. 1–10 Available at: http://www.cire.pl/pliki/1/2017/crmf_2016_summary_report_print_version.pdf, Accessed date: 4 April 2016.
- [5] OWPB. Cost reduction monitoring framework 2016. UK. 2016 Available at: http://www.cire.pl/pliki/1/2017/crmf_2016_summary_report_print_version.pdf, Accessed date: 17 August 2017.
- [6] Baringa. An analysis of the potential outcome of a further ‘Pot 1’ CfD auction in GB - a report for Scottish Renewables 2017 Available at: <https://www.scottishrenewables.com/publications/baringa-sr-analysis-potential-outcome-pot-1-cfd/>.
- [7] Leblanc C., Houlsby GT, Byrne BW. Response of stiff piles in sand to long-term cyclic lateral loading. Geotechnique 2010;60(2):79–90. <http://dx.doi.org/10.1680/geot.7.00196>.
- [8] Kallehave D, Byrne BW, LeBlanc Thilsted C, Mikkelsen KK. Optimization of monopiles for offshore wind turbines. Philosophical transactions. Series A, Math Phys Eng Sci 2015;373:1–15. <http://dx.doi.org/10.1098/rsta.2014.0100>.
- [9] Brennan FP. A framework for variable amplitude corrosion fatigue materials tests for offshore wind steel support structures. Fatig Fract Eng Mater Struct 2014;37(7):717–21. <http://dx.doi.org/10.1111/fe.12184>.
- [10] Bak C, Zahle F, Bitsche R, Yde A, Henriksen LC, Nata A, et al. Description of the DTU 10 MW reference wind turbine department of wind energy I-Report 2013 Available at: <https://dtu-10mw-rwt.vindenergi.dtu.dk>.
- [11] AMSC. SeaTitan 10 MW wind turbine. 2012. p. 2 Available at: <http://www.amsc.com/documents/seatitan-10-mw-wind-turbine-data-sheet/>.
- [12] Polinder H, et al. 10 MW wind turbine direct-drive generator design with pitch or active speed stall control. Proceedings of IEEE international electric machines and drives conference, IEMDC 2007 vol. 2. 2007. p. 1390–5. <http://dx.doi.org/10.1109/IEMDC.2007.383632>.
- [13] Freyd L, Dahlhaug OG. Rotor design for a 10 MW offshore wind turbine. International offshore and polar engineering conference vol. 8. 2011. p. 327–34.
- [14] 4 Coffshore. SWAY 10 MW (onshore) test turbine offshore wind farm. 2016 Available at: <http://www.4coffshore.com/windfarms/SWAY-10MW-test-turbine-Norway-No17.html>, Accessed date: 9 April 2016.
- [15] TII Group-Scheuerle. 1300 tonnes – world's largest monopile - Scheuerle. TII Ggroup-Scheuerle; 2016 Available at: <https://www.scheuerle.com/communication/press/press-releases/detail/getarticle/News/detail/1300-tonnes-worlds-largest-monopile-1.html>, Accessed date: 7 September 2017.
- [16] Dillinger. Offshore windpark “Gemini” stands on steel from Dillinger. Dillinger; 2017 Available at: <https://www.dillinger.de/d/en/news/press-releases/one-of-the-largest-in-the-world-77269.shtml>, Accessed date: 8 September 2017.
- [17] Yu LQ, Wang LZ, Guo Z, Bhattacharya S, Nikitas G, Li LL, et al. Long-term dynamic behavior of monopile supported offshore wind turbines in sand. Elsevier Ltd Theor Appl Mech Lett 2015;5(2):80–4. <http://dx.doi.org/10.1016/j.taml.2015.02.003>.
- [18] (DNV) Det Norske Veritas. DNV-RP-C203: fatigue design of offshore steel structures. Recommended practice DNV-RPC203. 2011 Available at: <ftp://128.84.241.91/tmp/MSE-420/Fatigue-Design-Offshore.pdf>.
- [19] Bhattacharya S, Nikitas N, Garnsey J, Alexander NA, Cox J, Lombardi D, et al. Observed dynamic soil-structure interaction in scale testing of offshore wind turbine foundations. Soil Dyn Earthquake Eng Elsevier 2013;54:47–60. <http://dx.doi.org/10.1016/j.soildyn.2013.07.012>.
- [20] Lombardi D, Bhattacharya S, Muir Wood D. Dynamic soil-structure interaction of monopile supported wind turbines in cohesive soil. Soil Dyn Earthquake Eng Elsevier 2013;49:165–80. <http://dx.doi.org/10.1016/j.soildyn.2013.01.015>.
- [21] Harte M, Basu B, Nielsen SRK. Dynamic analysis of wind turbines including soil-structure interaction. Elsevier Ltd Eng Struct 2012;45:509–18. <http://dx.doi.org/10.1016/j.engstruct.2012.06.041>.
- [22] Bhattacharya S, Adhikari S. Experimental validation of soil-structure interaction of offshore wind turbines. Soil Dynam Earthq Eng 2011;31(5–6):805–16. <http://dx.doi.org/10.1016/j.soildyn.2011.01.004>.
- [23] Bhattacharya S. Challenges in design of foundations for offshore wind turbines. Engineering & Technology Reference 2014. p. 1–9. <http://dx.doi.org/10.1049/etr.2014.0041>.
- [24] Vestas Wind Systems A/S. Vestas V120 4.5 MW wind turbine. Denmark. 2005 Available at: http://www.nrg-systems.hu/dok/en/V120_UK.pdf.
- [25] Bhattacharya S, Cox JA, Lombardi D, Wood DM. Dynamics of offshore wind turbines supported on two foundations. Proc Inst Civ Eng Geotech Eng 2013;166(2):159–69. <http://dx.doi.org/10.1680/geng.11.00015>.
- [26] Desmond C, Murphy J, Blonk L, Haans W. Description of an 8 MW reference wind turbine. 753(September). J Phys Conf 2016:092013 <http://dx.doi.org/10.1088/1742-6596/753/9/092013>.
- [27] DNV/Riso. Guidelines for design of wind turbines. Det Norske Veritas: Wind Energy Department87-550-2870-5; 2002, Accessed date: 5 April 2016.
- [28] Thorpe TW, Scott PM, Rance A, Silvester D. Corrosion fatigue of BS4360:50D structural-steel in seawater. Int J Fatig 1983;5(3):123–33.
- [29] Milella PP. Fatigue and corrosion in metals. Milan: Springer-Verlag; 2013. p. 529–30. <http://dx.doi.org/10.1007/978-88-470-2336-9>.
- [30] World sea temperature. United Kingdom sea temperatures. Seatemperature.Org; 2017 Available at: <https://www.seatemperature.org/europe/united-kingdom/>, Accessed date: 4 November 2017.
- [31] Vestas Wind Systems A/S. Vestas V164-8.0MW. 2011. p. 8. ce:doi:10/2012-EN.
- [32] Borgen E. Drivetrain concepts for wind: introduction of the sway turbine ST10. IQPC 3rd international conference. Swissôtel bremen. 2012 Available at: http://www.sway.no/publish_files/Sway_Turbine_presentation_22_October_2012.
- [33] Gilbert Nick. Structural steel - S235, S275, S355 chemical composition, mechanical properties and common applications. 2012 Available at: <http://www.azom.com/article.aspx?ArticleID=6022>, Accessed date: 30 July 2016.
- [34] Steel International T. New Horizons - supply solutions in offshore structural steel. 2010 Available at: http://www.tatasteeleurope.com/static_files/StaticFiles/Business_Units/International/Tata/Steel%20International%20Offshore%20Capability%202010.pdf, Accessed date: 5 April 2016.
- [35] Corus Construction & Industrial. European structural steel standard EN 10025 : 2004. 2004 Available at: http://www.tf.uni-kiel.de/matlis/amat/iss/kap_9/articles/en_stell_standards.pdf, Accessed date: 5 April 2016.
- [36] Tata Steel. Advance sections. 2013 Available at: http://www.tatasteeleurope.com/file_source/StaticFiles/section_plates/publications/sections_publications/Advance_to_Eurocode_Sect_13.pdf.
- [37] Parker Steel Company. S355 EN 10025: standard structural steel products. 2012 Available at: http://www.metricmetal.com/products/Grade_Descriptions/S355_Grade_Description.php, Accessed date: 1 April 2016.
- [38] Regency Steel Asia. EN 10225 chemical & mechanical properties. 2016 Available at: <http://www.regencysteelasia.com/pdf/pdf3.pdf>, Accessed date: 11 April 2016.
- [39] Tata Steel International. Product range - global steel supply and services. 2010 Available at: http://www.tatasteeleurope.com/file_source/StaticFiles/Business_Units/International/TATA_Product_Range_10_Update.pdf, Accessed date: 10 March 2016.
- [40] Nippon Steel & Sumitomo Metal. Steel plates for offshore structures Available at: https://www.nssmc.com/product/catalog_download/pdf/A003en.pdf; 2014.
- [41] MEADinfo. Material properties of S355 steel - an overview. 2015 Available at: <http://www.meadinfo.org/2015/08/s355-steel-properties.html>, Accessed date: 11 April 2016.
- [42] Dillinger. Thermomechanically rolled fine-grained steels. 2016 Available at: <https://www.dillinger.de/d/en/products/heavyplate/thermomechanically-finegrained/>, Accessed date: 11 April 2016.
- [43] Jaske CE, et al. Corrosion fatigue of structural steels in seawater and for offshore applications. Corrosion-fatigue technology, ASTM STP 652. 1978. p. 19–47.
- [44] Ruukki. Hot-rolled Steel PlateS, SHetS and CoilS Standard steel grades, comparison, designations and codes. 2011 Available at: <http://www1.ruukki.com/~media/Files/Steel-products/Hot-rolled-standard-steels/Ruukki-Hot-rolled-steels-Standard-steel-grades-comparison-designation-and-codes1.pdf>, Accessed date: 11 April 2016.
- [45] ASTM. ASTM E647-15: standard test method for measurement of fatigue crack growth rates. 2015. <http://dx.doi.org/10.1520/E0647-15.2>.

- [46] Mehanparast A, Brennan F, Tavares I. Fatigue crack growth rates for offshore wind monopile weldments in air and seawater: SLIC inter-laboratory test results. Mater Des 2017;114:494–504. <http://dx.doi.org/10.1016/j.matdes.2016.10.070>.
- [47] ASTM. D1141-98 standard practice for the preparation of substitute ocean water. Astm 2013;98(Reapproved):1–3. <http://dx.doi.org/10.1520/D1141-98R13.2>.
- [48] Adedipe O, Brennan F, Kolios A. Corrosion fatigue load frequency sensitivity analysis. Elsevier Ltd Marine Struct 2015;42:115–36. <http://dx.doi.org/10.1016/j.marstruc.2015.03.005>.
- [49] British Standards Institution. BS ISO 4965-2:2012-Metallic materials — dynamic force calibration for uniaxial fatigue testing Part 2: dynamic calibration device (DCD) instrumentation. 2012 Available at: <https://shop.bsigroup.com/ProductDetail/?pid=000000000030278819>, Accessed date: 25 September 2017.
- [50] British Standard. Corrosion of metals and alloys — corrosion fatigue testing —. British Standard; 2008.
- [51] Dhinakaran S, Prakash RV. Effect of low cyclic frequency on fatigue crack growth behavior of a Mn – Ni – Cr steel in air and 3. 5 % NaCl solution. Mater Sci Eng, A 2014;609:204–8. <http://dx.doi.org/10.1016/j.msea.2014.05.001>.
- [52] Vishay. Errors due to misalignment of strain gages single gage in a TN-511 errors due to misalignment of strain gages. 2010.
- [53] Vishay. Instruction bulletin B-127-14: strain gauge installations with M-Bond 200 adhesive. 2014 Available at: www.micro-measurements.com.
- [54] Vishay. Surface preparation for strain gauge bonding: application Note B-129-8. 2009 Available at: <http://ww2.bse.vt.edu/kumar/Instrumentation/StrainGauge/>.
- [55] Vishay. Techniques for attaching leadwires to unbonded strain gages TT-608 techniques for attaching leadwires to unbonded strain gages. 2010.
- [56] Vishay. Leadwire attachment techniques for obtaining maximum fatigue life of strain gages. 2012.
- [57] Vishay. Vishay m-m. Model P3 strain indicator and recorder. 2005 (March). Available at: <http://www.vishaypg.com/micro-measurements/>.
- [58] TML. TML strain gauges. Tokyo, Japan. 2015 Available at: www.tml.jp/e.
- [59] Vishay. Instruction bulletin B-147-5 application of m-coat J protective coating instruction bulletin B-147-5. 2015.
- [60] BSI. BS ISO 12108:2012, Metallic materials — fatigue testing — fatigue crack growth method. 2012.
- [61] Tavares I, Brennan F. The SLIC project. 2015 Available at: <http://www.ewea.org/offshore2015/conference/allposters/PO081.pdf>.
- [62] BSI Standards. BS 7910:2013+A1: guide to methods for assessing the acceptability of flaws in metallic structures. BSI Standards; 2015.
- [63] Scott PM, Thorpe TW, Silvester DRV. Rate-determining processes for corrosion fatigue crack growth in ferritic steels in seawater. Corrosion Sci 1983;23(6):559–75.
- [64] De Jesus AMP, Matos R, Fontoura BFC, Rebelo C, Simões Da Silva L, Veljkovic M. A comparison of the fatigue behavior between S355 and S690 steel grades. Elsevier Ltd J Construct Steel Res 2012;79:140–50. <http://dx.doi.org/10.1016/j.jcsr.2012.07.021>.
- [65] Tsay LW, Chern TS, Gau CY, Yang JR. Microstructures and fatigue crack growth of EH36 TMCP steel weldments. Int J Fatig 1999;21(8):857–64. [http://dx.doi.org/10.1016/S0142-1123\(99\)00021-3](http://dx.doi.org/10.1016/S0142-1123(99)00021-3).